Prospective grading of neoplastic change in rat esophagus epithelium using angle-resolved low-coherence interferometry

Adam Wax
John W. Pyhtila
Robert N. Graf
Duke University
Department of Biomedical Engineering
Durham, North Carolina 27708
E-mail: a.wax@duke.edu

Ronald Nines
The Ohio State University
Comprehensive Cancer Center
Columbus, Ohio 43210

Charles W. Boone
National Cancer Institute
Division of Cancer Prevention
Bethesda, MD 20892-7322

Ramachandra R. Dasari
Michael S. Feld
Massachusetts Institute of Technology
G. R. Harrison Spectroscopy Laboratory
Cambridge, Massachusetts 02139-4307

Vernon E. Steele
National Cancer Institute
Division of Cancer Prevention
Bethesda, MD 20892-7322

Gary D. Stoner
The Ohio State University
Comprehensive Cancer Center
Columbus, Ohio 43210

Abstract. Angle-resolved low-coherence interferometry (a/LCI) is used to obtain quantitative, depth-resolved nuclear morphology measurements. We compare the average diameter and texture of cell nuclei in rat esophagus epithelial tissue to grading criteria established in a previous a/LCI study to prospectively grade neoplastic progression. We exploit the depth resolution of a/LCI to exclusively examine the basal layer of the epithelium, approximately 50 to 100 μm beneath the tissue surface, without the need for exogenous contrast agents, tissue sectioning, or fixation. The results of two studies are presented that compare the performance of two a/LCI modalities. Overall, the combined studies show 91% sensitivity and 97% specificity for detecting dysplasia, using histopathology as the standard. In addition, the studies enable the effects of dietary chemopreventive agents, difluoromethylornithine (DFMO) and curcumin, to be assessed by observing modulation in the incidence of neoplastic change. We demonstrate that a/LCI is highly effective for monitoring neoplastic change and can be applied to assessing the efficacy of chemopreventive agents in the rat esophagus. © 2005 Society of Photo-Optical Instrumentation Engineers. [DOI: 10.1117/1.2102767]

1 Introduction

New avenues for monitoring cancer progression based on optical imaging techniques are under development using small animal models.[1–3] Such techniques employ fluorescent tags that exhibit preferential uptake by tumors. However, interactions between fluorescent tags and experimental therapeutics, such as potential chemopreventive agents, are unknown and may limit the applicability of these imaging techniques. The use of intrinsic contrast mechanisms, such as those used in light-scattering techniques, can circumvent these difficulties and provide a useful alternative for monitoring cancer progression.

Recently, light-scattering techniques were shown to be capable of detecting neoplastic transformation in animal models.[4,5] These techniques utilize the interaction between light and cellular structures to obtain quantitative information on nuclear morphology[4] or tissue micro/nanoarchitecture[5] in epithelial layers without the need for biopsy and histopathologic evaluation. These noninvasive, nonperturbative techniques provide a unique opportunity to study the biology of neoplastic progression in living tissue, free from artifacts associated with preparation of histopathological slides for diagnostic evaluation, and at times before the tumors become visible.

Presented here is a prospective study using angle-resolved low-coherence interferometry (a/LCI), a light-scattering technique, to monitor neoplastic progression through measure-

Address all correspondence to Adam Wax, Biomedical Engineering, Duke University, Box 90281, Durham, NC 27708. Tel.: (919) 660-5143; Fax: (919) 684-4488; E-mail: a.wax@duke.edu

ments of nuclear morphology.[4,6] The a/LCI technique obtains nuclear structural information by examining the angular distribution of backscattered light. With a/LCI, depth resolution is achieved by the use of a short-coherence-length light source in an interferometry scheme. This method of coherence gating is also employed to obtain depth resolution in optical coherence tomography (OCT), a technique used to construct tomographic images of living tissues.[7,8] However, a/LCI has the added feature of resolving the angular distribution of scattered light, enabling structural measurements that exceed the resolution obtained with OCT. In a/LCI measurements, just as in OCT, the depth resolution serves as a powerful means of rejecting multiply scattered light, enabling selective measurements of light that has interacted only with a tissue region of interest. This capability has been exploited to examine exclusively the morphology of basal cell nuclei, rejecting the light scattered by the suprabasal layers.

In the presented studies, quantitative measurements of nuclear morphology were used as biomarkers for detecting and characterizing the degree of neoplastic change in the rat esophagus. Two a/LCI systems are used to measure *in situ*, the mean diameter of cell nuclei and to parameterize the cytonuclear texture of cells in living tissue of rat esophageal epithelium without the need for fixation, sectioning, and staining. The mean diameter results, a measure of the degree of neoplastic transformation, are used to classify the tissue sites in a prospective fashion based on grading criteria established in a previous a/LCI study.[4] The performance of a/LCI to prospectively grade the tissue sites is compared with the observed modulation of the incidence of dysplasia used to assess the efficacy of chemopreventive agents.

2 Materials and Methods

2.1 Chemicals

NMBA, with a purity of $>99\%$ was purchased from Ash Stevens, Inc. (Detroit, Michigan) and solubilized in 20% dimethyl sulfoxide (DMSO). α-Difluoromethylornithine (DFMO) was obtained from the NCI DCPC Repository (c/o McKesson BioServices, Rockville, Maryland). DMSO and curcumin were purchased from Sigma Aldrich Chemical Company (Milwaukee, Wisconsin) and LKT Laboratories (St. Paul, Minnesota), respectively.

2.2 Animals and Housing

All of the experimental protocols were in accordance with National Institutes of Health (NIH) guidelines and approved by the Institutional Animal Care and Use Committees of Duke University, the Massachusetts Institute of Technology (MIT), and the Ohio State University (OSU). Male F344 rats, 4 to 5 weeks of age, were obtained from Harlan Sprague Dawley (Indianapolis, Indiana) and housed at OSU. The animals were kept three per cage at $20\pm2\,°C$ ambient temperature, $50\pm10\%$ relative humidity, and in a 12-h light/dark cycle. Twice weekly cage changes ensured maintenance of hygienic conditions. The animals were allowed to acclimate to the facility for 2 weeks before randomization into experimental treatment groups. The diet consisted of modified AIN-76A containing 20% casein, 0.3% D,L-methionine, 52% cornstarch, 13% dextrose, 5% cellulose, 5% corn oil, 3.5% AIN salt mixture, 1.0% AIN vitamin mixture, and 0.2% choline

bitartrate (Dyets, Bethlehem, Pennsylvania). Yellow lights were used in rooms where the animals were housed, since the chemopreventive agent, DFMO, is light sensitive. Food and water were available *ad libitum*.

2.3 Experimental Protocol

Carcinogen-treated animals (Table 1; groups 2, 3, 6, and 7) were given subcutaneous injections of NMBA (0.25 mg/kg body weight) in the intrascapular region three times a week for 5 weeks with concentrations adjusted weekly based on average body weight. The solvent for NMBA was 20% $DMSO:H_2O$ and the injection volume was 0.2 ml. Control groups (groups 1 and 5) received a similar injection regimen of 20% $DMSO:H_2O$. At 8, 12, and 20 weeks after the initial injection of NMBA, NMBA-treated and control rats were shipped to MIT (DFMO studies) or Duke University (curcumin studies) to be harvested for optical spectroscopic analysis. The rats were euthanized by CO_2 asphyxiation and subjected to gross necropsy. The entire esophagus was excised and opened longitudinally for immediate optical spectroscopic analysis. Following spectroscopic analysis, the esophagus was fixed in 10% neutral buffered formalin.

2.4 Chemopreventive Agents

Selected groups of rats were fed the chemopreventive agents, DFMO (1000 ppm, groups 3 and 4) or curcumin (6000 ppm, groups 7 and 8) in modified AIN-76A diet beginning 1 week after cessation of NMBA treatment until the time of analysis. The diets containing DFMO or curcumin were prepared weekly and stored at $4\,°C$ before administration to the animals. The concentrations of DFMO and curcumin in the diets were confirmed by high-performance liquid chromatography (HPLC).

2.5 Angle-Resolved Low-Coherence Interferometry

Intact *ex vivo* tissue samples were examined using the a/LCI technique, implemented in one of two modalities. Samples from the DFMO study (groups 1 to 4) were examined using the original a/LCI prototype (Fig. 1) based on a modified Michelson interferometer geometry, which used a superluminescent diode (SLD) ($\lambda_0=845$ nm, FWHM bandwidth 22 nm) as a light source.[9,10] Light from the SLD is divided by a beamsplitter (BS) into a reference beam and an input beam to the sample. The reference beam is reflected by a mirror (M) and recombined at BS with light reflected by the sample. The mixed fields generate an interference pattern provided that the two optical path lengths are matched to within the coherence length of the source ($l_c=2\ln2/\pi\times\lambda^2/\Delta\lambda=14.3\ \mu$m). A heterodyne signal is generated by translating the reference mirror (M) at a constant velocity (4 mm/s), resulting in an oscillation in the heterodyne signal at the corresponding Doppler-shifted frequency (9.5 kHz). The beat intensity is determined by calculating the power spectrum of the digitized photocurrent (sampled at 333 kHz) and bandpassing the signal at the heterodyne frequency.

The original prototype a/LCI system uses four achromatic imaging lenses (L1 to L4, focal lengths f_1 to f_4) to enable the measurement of angular scattering distributions. These lenses are arranged to form multiple $4f$ imaging systems, which image both the phase and amplitude of the light field. The ref-

Table 1 Protocol for administration of NMBA and chemopreventives in the a/LCI study of chemopreventive efficacy in the rat esophagus epithelium.

Group	Treatment	Dose (mg/kg body weight)	Diet	Number of Rats Sacrificed at		
				8 weeks	12 weeks	20 weeks
1	DMSO+ H$_2$O	0	AIN-76A	5	3	3
2	NMBA	0.25	AIN-76A	5	5	5
3	NMBA	0.25	AIN-76A+ DFMO (1000 ppm) weeks 6 to 25	5	7	7
4	None	0	AIN-76A+ DFMO (1000 ppm) weeks 6 to 25	5	5	1
5	DMSO+ H$_2$O	0	AIN-76A	—	3	1
6	NMBA	0.25	AIN-76A	—	3	3
7	NMBA	0.25	AIN-76A+ curcumin (6000 ppm) weeks 6 to 25	—	3	3
8	None	0	AIN-76A+ curcumin (6000 ppm) weeks 6 to 25	—	3	3

erence field is made to cross the detector plane at a variable angle by scanning lens L2 (f_2=4.5 cm) a distance Δy perpendicular to the beam path. It can be shown using Fourier optics that this translation causes the reference field to be reproduced in the plane of the detector (D) with its angle of propagation changed by $\theta_T = 2\Delta y / f_2$ but its position unchanged.[10]

Samples from the curcumin study (groups 5 to 8) were probed using a new, second-generation a/LCI system (Fig. 2) based on a Mach-Zehnder interferometer, which used a mode-locked Ti:sapphire laser (λ_0=830 nm, FWHM bandwidth 10 nm) as a light source. The light is split into signal and reference fields by a beamsplitter and offset in frequency using acousto-optic modulators (AOMs), resulting in a heterodyne beat signal of 10 MHz when the two fields are mixed at beamsplitter BS2. By exploiting the short coherence length (30 μm) of the source, the detected signal field can be resolved by its optical path length. To obtain information about the signal field at various depths within a sample, a retroreflector (RR) has been included in the reference beam path to vary its path length by 2 Δz. The system uses a balanced detector (D1 and D2, New Focus Model 1807), with the pho-
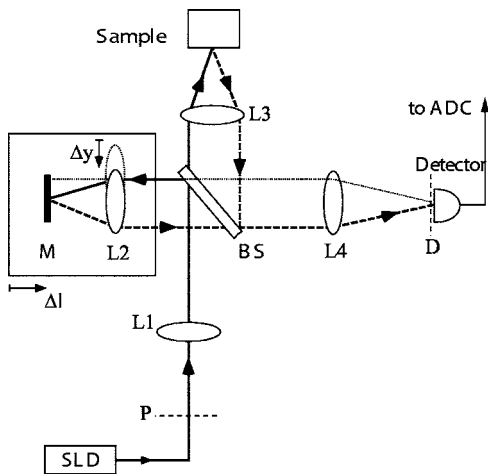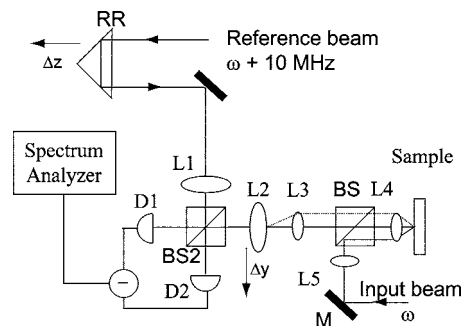

Fig. 1 Schematic of original prototype a/LCI system. The displacement of lens L2 causes the angle that the reference beam crosses the detector plane to vary.

Fig. 2 Schematic of second generation a/LCI system. The displacement of lens L2 causes the scattering angle, which overlaps the reference beam to vary.

tocurrent demodulated using a spectrum analyzer (HP 8594E) resulting in better SNR and faster acquisition times while offering the same precision and accuracy for obtaining structural information.[11]

The second-generation system measures the angular distribution of the scattered field by scanning lens L2 a distance Δy perpendicular to the beam path. It has been shown using Fourier optics that this translation will enable selective detection of the light that arrives at the plane of L2 traveling at an angle $\theta = \Delta y / f_2$ relative to the optical axis, where $f_2 = 10$ cm is the focal length[12] of L2. Lens L1 ($f_1 = 10$ cm) is included to alter the wavefront of the reference field to compensate for the effects of L2. Lenses L3 and L4 form a $4f$ system, imaging both the phase and amplitude of the scattered field onto the plane of lens L2. Lens L5 ($f_5 = 10$ cm) is included so that L4 does not focus the input beam on the sample, but instead recollimates it into a pencil beam.

Measured a/LCI data from both systems consist of the angular distribution of scattered light, which contains information about the tissue structure, as a function of depth within the tissue. The light scattered from a particular depth is selectively detected using coherence gating. The effects of scattering by layers superficial to those of interest have been discussed previously[10] and are negligible for a typical depth of 50 to 80 μm selected for analysis in these studies, which corresponds to the basal cell layer of the esophageal epithelium. The basal layer is identified by the topmost sharp peak in the density profile of the tissue, obtained by integrating the a/LCI data over angle. Note that a thickened keratin layer is observed for dysplastic samples, which can cause the basal layer to be as deep as 200 μm (Figs. 3 and 4). Although multiple scattering is more significant at these depths, previous studies have shown that the oscillations in the angular distribution used to determine size are still evident,[10] in agreement with the presence of angular oscillations in the current data.

The diameter of the probe beam, approximately 400 μm with both systems, enables a few hundred cells to be sampled at once, providing an average nuclear morphology measurement within the probe volume. The use of an average minimizes the effect of cell-to-cell variations in nuclear morphology such as irregular nuclear shape and variations in density arising from differing phases of the reproductive cycle. The depth of the basal layer may be modulated by tens of micrometers over the relatively broad diameter of the probe beam. In such cases, the topmost peak corresponding to the basal layer is broadened, spanning up to 50 μm in cases of HGD (Figs. 3 and 4). To accommodate such variations, the imaging depth selected for analysis is chosen to span the full width at half maximum of the topmost peak.

The a/LCI data from the basal cell layer of each sample was processed and analyzed to determine the mean diameter of the cell nuclei, as previously described.[6] In brief, a/LCI data consist of an oscillatory component superposed on a slowly varying background. The slowly varying feature of the a/LCI data was modeled using a second-order polynomial and removed. The resulting oscillatory component was then compared to a database of theoretical predictions obtained using Mie theory from which the slowly varying features were similarly removed for analysis. The theoretical predictions were calculated for a Gaussian distribution of sizes characterized by a mean diameter (d) and standard deviation (δD). In addition, the refractive index of the nuclei relative to the cytoplasm was varied from 1.015 to 1.072 in 36 discrete steps. The a/LCI technique is most sensitive to changes in mean nuclear diameter, the descriptor of nuclear morphology used in this study; however, useful information may also be obtained from the standard deviation (δD) and refractive index measurements.

On obtaining the nuclear size distribution, the complete Mie theory prediction for the determined size distribution was subtracted from the measured a/LCI data. The resulting background component was then Fourier transformed to yield the two point correlation function, $\Gamma(r)$, with r as the correlation distance. The general form of $\Gamma(r)$ for the tissue samples was a power law of the form $1/r^\alpha$, as indicated by its appearance as a straight line on a log-log plot. The parameter α was determined by a least squares fit to the data and related to the fractal dimension (FD) of these structures[6] by $\alpha = 3$ FD. The use of the FD provides a physical interpretation of this measurement as the texture of the subcellular components.[13] A larger FD corresponds to a denser, grainier distribution of structures, whereas a smaller FD indicates a smoother, finer distribution. For each sample, both the mean diameter of the cell nuclei and the FD are reported.

The a/LCI measurements of mean nuclear diameter are compared to grading criteria established using logistic regression in the first retrospective a/LCI study of the rat esophagus carcinogenesis (REC) model[4] and classified as normal ($7.5 \leqslant d \leqslant 10.2$ μm), LGD ($10.2 < d \leqslant 13.5$ μm), HGD ($d > 13.5$ μm), or apoptotic ($d < 7.5$ μm). Representative a/LCI data obtained using the original prototype and second generation systems are shown for each classification in Figs. 3 and 4, respectively.

2.6 Tumor Metrology, Histological Processing, and Grading of Neoplastic Tissues

Prior to a/LCI analysis, the entire esophagus of each rat was excised, opened longitudinally, and lesions (tumors) $\geqslant 0.05$ mm in a single dimension were counted, mapped and measured. Tumor volume was calculated using the formula: length $\times$ width $\times$ height.

Following the a/LCI scan, the flat strip of the each esophagus was cut laterally into thirds. Each strip was paraffin embedded with the epithelium uppermost. Longitudinal sections of each esophagus were cut (thickness, 4 μm), mounted on a microscope slide and stained with hematoxylin and eosin (H&E). The tissue site corresponding to the area scanned using a/LCI was identified by measuring its location relative to the muscle gap at the tracheal junction of the esophagus. For the DFMO studies, a single tissue site, located 5 mm distal to the muscle gap and laterally centered, was probed on each sample with a/LCI. For the curcumin studies, the use of the new a/LCI system enabled multiple tissue sites on each sample to be probed. The additional probed sites were located distal to the first site, in increments of 1 mm along the lateral center. Each probed tissue site was classified histologically as follows: normal epithelium, LGD, HGD, or epithelium with apoptotic cells (Fig. 1). This classification scheme was based on microscopic descriptions of dysplasia and apoptosis given in Cotran et al.[14]
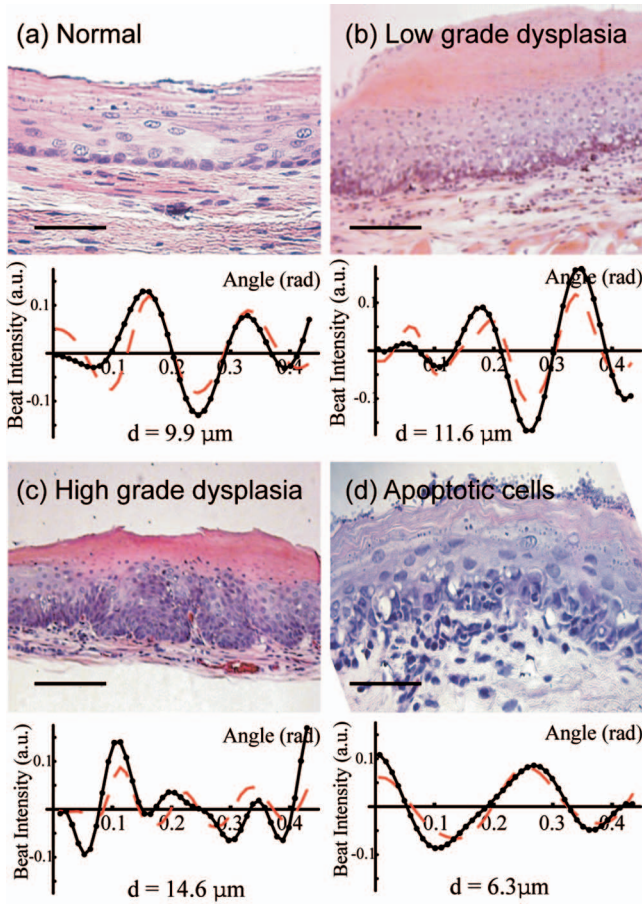
Fig. 3 Typical a/LCI data (solid line) obtained with the original prototype system shown for each of the histological classifications. The mean size of the basal cell nuclei, as determined from the best fit to the data (dashed line), is given below. Photomicrographs of fixed and stained esophagus sections illustrate the classification scheme [bar =25 mm for (a),(d); bar=100 mm for (b),(c)]. Typical example of (a) normal epithelium, (b) low-grade dysplasia (LGD), (c) high-grade dysplasia (HGD), and (d) epithelium with apoptotic bodies.

Fig. 4 Typical a/LCI data (solid line) obtained with the second generation system are shown for each of the histological classifications. The mean size of the basal cell nuclei, as determined from the best fit to the data (dashed line), is given below. Photomicrographs of fixed and stained esophagus sections illustrate the classification scheme [bar=100 mm for (a) to (d)]. Typical example of (a) normal epithelium, (b) LGD, (c) HGD, and (d) epithelium with apoptotic bodies.

3 Results

3.1 *DFMO Study*

The DFMO study used a/LCI to probe the nuclear morphology of the rat esophagus epithelium samples at 8, 12, and 20 weeks after the first NMBA injection. For each probed tissue site, the mean nuclear diameter was compared to the grading criteria to make a classification, as described above. The classification results are presented in Table 2. At each time point, the number of samples for each classification for each animal group as defined in Table 1 are shown. For each classification, the average of the mean nuclear diameter measurements, as well as the average fractal dimension are given in Table 2.

At 8 weeks after the first NMBA injection, the average of the mean nuclear diameter measurements for normal tissue sites is 8.95 ± 0.76 μm and increases to 11.2 μm for the two LGD sites. No HGD or apoptotic sites were detected. Note that for the limited number of LGD sites found at this time point, the standard deviation is not meaningful. Standard deviations will be given only for average measurements that
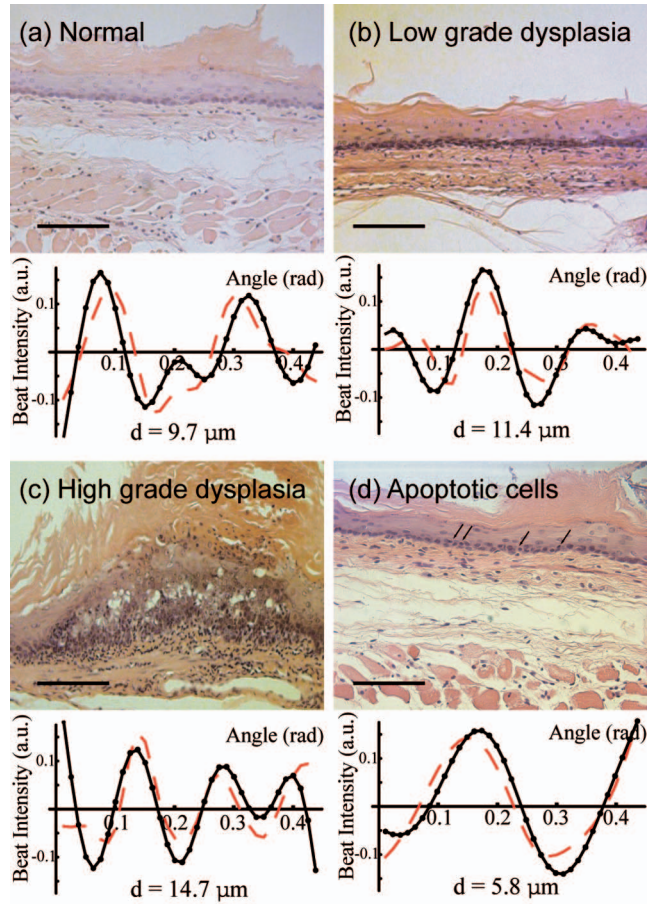
include three or more sites. An increase in FD with neoplastic progression is also observed. The mean FD of the normal tissue sites at 8 weeks was found to be 1.91 ± 0.32 and increased to 2.05 for the LGD tissues, a difference that did not reach statistical significance ($p=0.1$ with Student t test, used for all statistical analysis here).

At 12 weeks after the first NMBA injection, the average of the mean nuclear diameter measurements for normal tissue sites is 8.95 ± 1.4 μm and increases to 11.7 ± 0.53 μm for the LGD sites. Three apoptotic sites, with an average mean nuclear diameter measurement of 6.60 ± 0.60 μm, and no HGD sites were found. The FD was also found to increase with neoplastic progression, from 1.95 ± 0.24 for normal tissue sites to 2.17 ± 0.06 for the LGD tissue sites, a statistically significant difference ($p < 0.02$). The average FD of the three apoptotic samples was 2.12 ± 0.10, which is greater than that for normal tissues.

At 20 weeks after the first NMBA injection, the average of the mean nuclear diameter measurements for normal tissue sites is 9.70 ± 1.0 μm and increases to 11.0 μm for LGD sites and 13.9 μm for HGD sites. In addition, the tissue sites clas-

Table 2 Classification of rat esophagus tissue sites examined in the DFMO study at 8, 12 and 20 weeks.

Week 8

Group	Normal	LGD	HGD	Apoptotic
1 (Normal)	5	0	0	0
2 (NMBA only)	2	1	0	0
3 (NMBA+DFMO)	2	1	0	0
4 (DFMO only)	3	0	0	0
Total:	12	2	0	0
Mean diam. (μm)	8.95±0.76	11.2	x	x
FD	1.91±0.32	2.05	x	x

Week 12

Group	Normal	LGD	HGD	Apoptotic
1 (Normal)	2	0	0	0
2 (NMBA only)	2	5	0	0
3 (NMBA+DFMO)	2	0	0	2
4 (DFMO only)	3	0	0	1
Total:	9	5	0	3
Mean diam. (μm)	8.95±1.4	11.7±0.53	x	6.60±0.60
FD	1.95±0.24	2.17±0.06	x	2.12±0.10

Week 20

Group	Normal	LGD	HGD	Apoptotic
1 (Normal)	3	0	0	0
2 (NMBA only)	2	2	2	0
3 (NMBA+DFMO)	2	0	0	2
4 (DFMO only)	0	0	0	1
Total:	7	2	2	3
Mean Diam. (μm):	9.70±1.0	11.0	13.9	5.80±0.36
FD:	1.69±0.25	2.09	2.08	1.94±0.10

The number of tissue sites exhibiting the classification in each group, as defined in Table 1, is given. The summary shows the total number of each classification, the average FD and the average mean nuclear diameter for that class, with standard deviations given for classifications containing three or more samples.

sified as apoptotic had an average mean nuclear diameter measurement of 5.80±0.36 μm. The FD of the tissue sites was found to be 1.69±0.25 for the normal sites, 2.09 for the LGD, 2.08 for the HGD and 1.94±0.10 for the apoptotic tissue sites.

The tissue classifications in the prospective study presented here were determined by a/LCI measurements of mean

nuclear diameter using the original prototype system and confirmed by histopathological evaluation of the probed tissue sites to determine the accuracy of the a/LCI grading method. At each time point, it was typical for a small number of samples to present significant artifacts, which prevented coregistration of the two classification methods. Such samples have been omitted from Table 2, resulting in a discrepancy between the total numbers of samples compared to the groups presented in Table 1.

For samples where coregistration was achieved, the two classification methods were found to agree entirely for the 8-week samples. At 12 and 20 weeks, the a/LCI measurements classified one tissue site from each time point as LGD when histopathology indicated that they were normal, resulting in two false positives. When these results are taken into account, we find the original a/LCI system exhibited 100% sensitivity (11/11 dysplastic tissue sites) and 93% specificity (26/28 normal tissue sites) for detecting dysplastic tissues upon comparison to histopathology in the DFMO study.

To assess the efficacy of DFMO as a chemopreventive agent, we compare the incidence of dysplasia (LGD+HGD) for the group 2 (NMBA only) and group 3 (NMBA +DFMO) samples. At 8 weeks after the first NMBA injection, we find that the incidence of dysplasia is the same (33%), with one LGD site found in each group. However, at 12 weeks, a significant difference between the two was seen, with the group 2 samples showing a high incidence (71%) of dysplasia and no apoptotic samples and group 3 showing no incidence (0%) of dysplasia but with a significant number of apoptotic tissue sites (50%). This difference is also seen at 20 weeks, with a high incidence (57%) of dysplasia and no apoptotic sites found in group 2 and no incidence (0%) of dysplasia and a significant number of apoptotic sites (50%) in group 3.

The chemopreventive efficacy of DFMO can also be assessed by examining the tumor incidence, multiplicity and size data for the samples used in the study (Table 3). The data show no significant difference between the tumor metrology for group 2 (NMBA only) and group 3 (NMBA+DFMO) at 8 and 12 weeks after the first NMBA injection. Note that the tumor incidence, multiplicity and size actually are greater for group 3 compared to the measurements for group 2 but that the differences do not reach statistical significance ($P > 0.05$). At 20 weeks, the tumor incidence and tumor size are decreased for group 3 compared to group 2 but the tumor multiplicity is actually slightly increased. Of these differences, only the change in tumor size is statistically significant ($P < 0.005$).

Thus, for a/LCI analysis, we see no change in incidence at 8 weeks but a sharp decrease in incidence of dysplasia accompanied by an increase in apoptosis for DFMO treated samples at 12 and 20 weeks. In comparison, the tumor metrology data show no significant differences at 8 and 12 weeks but a statistically significant decrease in tumor size at 20 weeks.

3.2 Curcumin Study

The curcumin study used the second generation a/LCI system to probe nuclear morphology in the rat esophagus at 12 and 20 weeks after the first NMBA injection. For the a/LCI data

Table 3 Tumor incidence, multiplicity and size data for the samples used in the DFMO and curcumin studies.

DFMO Study: Group 2 (NMBA control)			
	Tumor Incidence (%)	Tumor Multiplicity (Mean)	Tumor Size (mm³)
Week 8	40	0.4	0.3
Week 12	80	1.8±0.2	4.8±2.4
Week 20	100	3.4±1.2	31.3±12.6
Group 3 (NMBA+DFMO)			
	Tumor Incidence (%)	Tumor Multiplicity (Mean)	Tumor Size (mm³)
Week 8	20	0.2	1.2
Week 12	100	2.2±0.5	9.0±3.1
Week 20	80	3.8±0.4	9.8±4.6
Curcumin Study: Group 6 (NMBA control)			
	Tumor Incidence (%)	Tumor Multiplicity (Mean)	Tumor Size (mm³)
Week 12	100	3.0±0.7	13.1±9.1
Week 20	100	2.7±0.5	7.7±4.3
Group 7 (NMBA+curcumin)			
	Tumor Incidence (%)	Tumor Multiplicity (Mean)	Tumor Size (mm³)
Week 12	66.7	0.7±0.4	4.5±0.0
Week 20	100	3.5±0.3	20.8±10.7[a]

Samples treated with DFMO show a statistically significant decrease ($P < 0.005$) in tumor size in comparison to that of untreated samples at 20 weeks. The only other statistically significant change is seen in the decrease in tumor multiplicity between curcumin treated and untreated samples at 12 weeks ($P < 0.02$).
[a]Includes one unusually large tumor; average drops to 9.4 ± 5.9 mm³ if omitted.

Table 4 Classification of rat esophagus tissue sites examined in the curcumin study at 12 and 20 weeks.

Week 12				
Group	Normal	LGD	HGD	Apoptotic
5 (Normal)	3	0	0	0
6 (NMBA only)	2	3	0	0
7 (NMBA+Curcumin)	4	2	0	1
8 (Curcumin only)	5	0	0	0
Total:	14	5	0	1
Mean diam. (mm)	8.89±0.55	12.5±1.5	×	6.40
FD	1.79±0.26	2.16±0.32	×	2.03
Week 20				
Group	Normal	LGD	HGD	Apoptotic
5 (Normal)	6	0	0	0
6 (NMBA only)	0	5	1	0
7 (NMBA+Curcumin)	5	0	0	0
8 (Curcumin only)	7	0	0	1
Total:	18	5	1	1
Mean diam. (μm)	8.71±0.43	11.1±1.4	14.7	5.80
FD	1.69±0.10	1.72±0.12	1.59	1.86

The number of tissue sites exhibiting the classification in each group, as defined in Table 1, is given. The summary shows the total number of each classification, the average FD and the average mean nuclear diameter for that class, with standard deviations given for classifications containing three or more samples.

obtained from each tissue site, the classification was determined by comparing the mean nuclear diameter to the grading criteria described above. Table 4 lists the number of samples for each classification in each group at 12 and 20 weeks. The average morphological parameters for each classification are also given.

At 12 weeks after the first NMBA injection, the average of the mean nuclear diameter measurements for normal tissue sites is 8.89 ± 0.55 μm. The average increases to 12.5 ± 1.5 μm for the LGD tissue sites. No HGD sites were detected at 12 weeks. For the one site classified as apoptotic, the mean nuclear diameter was found to be 6.40 μm with a FD of 2.03. The morphological parameters also reveal an increase of FD with neoplastic progression. The mean FD of the normal tissue sites at 12 weeks was found to be 1.79 ± 0.26 and increased to 2.16 ± 0.32 for the LGD tissues, a statistically significant difference ($p = 0.01$).

At 20 weeks after the first NMBA injection, the average of the mean nuclear diameter measurements for the normal tissue sites is 8.71 ± 0.43 μm. The average increases to 11.1 ± 1.4 μm for the LGD sites and the mean nuclear diameter determined for the one HGD site was 14.7 μm. A single apoptotic site with a mean nuclear diameter of 5.80 μm was observed. The FD was not seen to vary significantly with neoplastic progression with an FD of 1.69 ± 0.10 for normal tissue sites, 1.72 ± 0.12 for the LGD sites, and 1.59 for the single HGD tissue site. The FD of the apoptotic sample was found to be 1.86.

The tissue classifications presented in this section were determined by a/LCI measurements executed with the second generation system and subsequently confirmed by histopathological evaluation of the probed tissue sites. However, as shown in Table 1, fewer animals were used for the curcumin study than for the DFMO study. This decrease was enabled by the faster data acquisition time of the second generation a/LCI system, permitting up to six data points to be acquired from one tissue sample. As with the DFMO study, when the histological slides of the samples presented significant artifacts, which prevented coregistration with the a/LCI probe, the data

Table 5 Sensitivity and specificity obtained by comparing a/LCI diagnosis with the results of traditional histopatholgy.

a/LCI system	Sensitivity	Specificity
Original prototype	100% (11/11 dysplastic sites)	93% (26/28 normal sites)
Second generation	82% (9/11 dysplastic sites)	100% (32/32 normal sites)
Combined results	91%	97%

were omitted from the study. The consequences of discarding these data are described in the discussion section.

For samples where coregistration was achieved, the a/LCI and histopathological grading methods were found to completely agree for the 12-week samples. For the 20-week samples, a/LCI identified two LGD tissue sites as normal, resulting in two false negatives. To clarify this difference in grading, note that these two false negatives were found to have mean nuclear diameters of 10.2 μm, only 0.1 μm below decision line. Including these two false negatives, the use of the second-generation a/LCI system to prospectively grade the neoplastic progression of the tissue sites resulted in 82% sensitivity (9/11 dysplastic tissue sites) and 100% specificity (32/32 normal tissue sites).

To assess the efficacy of curcumin as a chemopreventive agent, we compare the incidence of dysplasia (LGD+HGD) for the group 6 (NMBA only) and group 7 (NMBA +curcumin) samples. For the 12-week data, there is a slight difference between group 6, showing a high (60%) incidence of dysplasia, and group 7, which shows a significantly lower incidence (29%) of dysplasia and some apoptotic sites (14%). The difference becomes more pronounced at 20 weeks, with a high incidence (100%) of dysplasia in group 6 and no incidence (0%) of dysplasia in group 7, although no apoptotic sites were detected for this group.

The chemopreventive efficacy of curcumin can also be assessed by examining the tumor incidence, multiplicity and size data for the samples used in the study (Table 3). The data show decreases in tumor incidence, multiplicity and size be-

Table 6 Trends in the mean nuclear diameter, given in micrometers, for tissue sites in the DFMO study are given.

Classification by Group	Week 8	Week 12	Week 20
Normals from groups 1 and 2 (no DFMO)	9.2	9.6	10.3[a]
Normal from groups 3 and 4 (DFMO)	8.7	8.5	8.4
Nondysplastic from groups 3 and 4 (DFMO)	8.7	7.8	6.8

Samples treated with DFMO show a decrease in mean nuclear diameter in comparison to mean nuclear diameter of untreated samples.
[a]Includes one false positive; average drops to 10.1 μm if omitted.

tween group 2 (NMBA only) and group 3 (NMBA +curcumin) at 12 weeks after the first NMBA injection. We note that only the decrease in tumor multiplicity has a statistical significance ($P<0.02$). At 20 weeks, none of the tumor data show decreases for group 3 compared to those for group 2 but the changes are not statistically significant ($P>0.05$).

Thus, with a/LCI analysis, we see a significant change in incidence of dysplasia at 12 weeks with a sharper decrease in incidence seen for curcumin treated samples at 20 weeks. In comparison, the tumor metrology data show significant decrease in tumor multiplicity at 12 weeks but no statistically significant decreases in any of the tumor metrology data at 20 weeks.

4 Discussion

In the two studies described here, a/LCI was used to prospectively grade the neoplastic progression of rat esophagus epithelium samples through nuclear morphology measurements carried out in freshly excised, intact tissue samples without the need for exogenous staining agents, fixation or tissue sectioning. The mean diameter of cell nuclei in the basal epithelial layer was used as the grading criteria, as it was shown to be a powerful indicator of neoplastic progression in a previous study.[4] The utility of a/LCI for monitoring neoplastic progression is evident by the high rate of success in classifying tissues by their degree of neoplastic change (Table 5). The original prototype a/LCI system exhibited a high sensitivity and specificity (100% and 93% respectively) while the second generation system also showed a lower sensitivity (82%) but a higher specificity (100%). We note that the decrease in sensitivity of the second-generation system is due to two false negatives seen in the sites examined at 20 weeks for which the measured diameter was only slightly below the decision line. Overall, on combining the results of the two studies, we find that a/LCI successfully identified 58 of 60 normal tissue sites (97% specificity) and 20 of 22 dysplastic tissue sites (91% sensitivity).

Analysis of the mean nuclear diameter data reveals an anomalous statistical trend in the standard deviation of the average mean nuclear diameter measurements for tissue sites classified as normal in the DFMO study. The average mean nuclear diameter is seen to change from 8.95 ± 0.76 μm at 8 weeks to 8.95 ± 1.4 μm at 12 weeks to 9.70 ± 1.0 μm at 20 weeks. On further examination, we can see that this trend is due to the emergence of a bimodal distribution of the mean nuclear diameters, as shown in Table 6. By separating the normal samples into those treated with DFMO and those without treatment, we see that the mean nuclear diameter in-
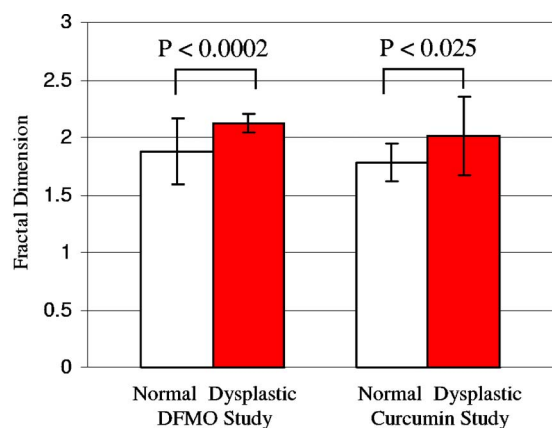
Fig. 5 Graphical comparison of the average fractal dimension of normal and dysplastic tissue sites for the DFMO and curcumin studies. In both studies, a statistically significant difference in the average fractal dimension was observed ($P<0.0002$ and $P<0.025$ for normal and dysplastic tissue sites, respectively).

creases with time for the untreated samples* (9.2 to 9.6 to 10.3 μm) and slightly decreases with time for samples treated with DFMO (8.7 to 8.5 to 8.4 μm). The decreasing trend of the treated samples becomes even clearer when all nondysplastic samples (normal+apoptotic) are combined (8.7 to 7.8 to 6.8 μm). The bimodal trend shows a manifestation of the chemopreventive action of DFMO, in that it causes changes in nuclear morphology that are consistent with the structural changes seen in apoptosis. Although these trends in nuclear size are not evident in the normal samples from the curcumin study, i.e., no distinct changes in the standard deviation are observed, the results of the DFMO study suggest that it may be appropriate to include the age of the animals and/or chemopreventive regimen in determining the decision lines used to classify tissues based on a/LCI measurements.

In addition to the mean nuclear diameter, we report on the fractal dimension of subcellular structures in the probed tissue sites (Fig. 5). Although this parameter was not used in grading the tissue sites, the FD has become an area of recent interest in animal models of carcinogenesis.[4,5] In the DFMO study, the normal tissue sites show an FD of 1.88 ± 0.29, whereas those classified as dysplastic show an FD of 2.12 ± 0.08, a statistically significant difference ($p<0.0002$). For the curcumin study, an FD of 1.78 ± 0.17 is obtained for normal tissue sites with an FD of 2.01 ± 0.34 seen for dysplastic sites, which is also a statistically significant difference ($p<0.025$), although not as great as in the DFMO study. These results are presented graphically in Fig. 5 and are consistent with our previous findings using this model[4] and those found for a study of the FD of precancerous rat colon epithelium.[5] In the a/LCI data, the change in the FD arises from corresponding changes in the structural composition of the cells and tissues in the 2- to 10-μm size range as they undergo neoplastic transformation. The correlation function $\Gamma(r)$ of the tissues reveals

that this change corresponds to a decrease in smaller structures and an increase in larger structures. This physical interpretation agrees nicely with changes in the texture of cell nuclei seen in histological images, where clumped, grainy cell nuclei are characteristic of dysplasia. Continued study of FDs in animal models may lead to an improved understanding of mechanisms of carcinogenesis, while improvements in FD measurements, which yield improved statistical significance,[5] will serve to increase its value as a diagnostic biomarker.

In addition to monitoring neoplastic transformation, one goal of the studies was to determine the efficacy of the chemopreventive agents by measuring changes in nuclear morphometry using a/LCI. In a previous study, we identified that chemopreventive action can be inferred by using a/LCI to detect the presence of apoptotic cells within the tissue.[4] This finding is corroborated by the identification of stimulation of apoptosis as the mechanism behind the efficacy of DFMO as a chemopreventive agent in rat esophagus epithelium.[15] For the tissue sites classified as apoptotic, the a/LCI measurements showed a decrease in mean nuclear diameter and an increase in FD, both features agreeing with the contracted nucleus seen in apoptosis. Both the DFMO and curcumin treated samples showed evidence of apoptotic cells, while simultaneously showing decreased incidence of dysplasia.

The capability of a/LCI to detect subtle changes in nuclear morphology enables greater sensitivity in assessing chemopreventive efficacy than traditional studies using tumor metrology data. In the DFMO study, a/LCI detects modulation in the incidence of dysplasia, accompanied by the presence of apoptotic cells as early as 12 weeks after the initial NMBA injection. The tumor metrology data, on the other hand, does not confirm the chemopreventive efficacy until 20 weeks, with the first appearance of statistically significant changes. Further, although the tumor data for the curcumin study shows a decrease in incidence and tumor multiplicity at 12 weeks, confirming the a/LCI findings, the limited number of samples in this study yields no statistically significant changes at 20 weeks. In these studies, the limited number of animals used per group (three to seven animals/group) affected the statistical significance of the tumor metrology data. (Note that the number of animals in these studies was far smaller than the 30 animals per group typically used for a classic bioassay.) Thus, we see that a/LCI can assess chemopreventive efficacy with fewer samples than conventional methods.

The sensitivity afforded by a/LCI enables a comparison of the relative chemopreventive efficacy of DFMO and curcumin by examining the frequency of the observed classifications. While DFMO produced a sharp decrease in the incidence of dysplasia at 12 and 20 weeks, accompanied by a significant number of sites with apoptotic cells, it was found that curcumin produced a milder decrease in both the incidence of dysplasia and apoptosis at 12 weeks. This suggests that at the dose levels tested, curcumin is not as effective as DFMO as a chemopreventive agent in the rat esophagus.

At 20 weeks, the decrease of incidence of dysplasia in the curcumin treated rats was similar in degree to that found for the DFMO treated rats. However, only 1 apoptotic tissue site out of 13 (1/13) was seen in the curcumin samples at 20 weeks, which was smaller than the number seen in the

---

*Note that the 10.3-μm measurement is above the decision line between normal and dysplastic tissues. This figure includes one false positive a/LCI measurement. On excluding the false positive, the average measurement falls to 10.1 μm.

DFMO samples (3/5) at 20 weeks. The decrease in incidence of apoptosis also supports the assertion that curcumin is not as effective a chemopreventive agent as DFMO at the tested dosage levels.

5 Conclusion

In summary, the utility of a/LCI measurements of nuclear morphology as biomarkers for monitoring neoplastic transformation has been demonstrated via a prospective study, obtaining high sensitivity and specificity with both instrument designs. The *in situ* nuclear morphology measurements are accomplished without the use of exogenous staining agents, fixatives, or tissue sectioning. The a/LCI technique was applied to determine the efficacy of DFMO and curcumin as chemopreventive agents in rat esophagus epithelium. Future applications of a/LCI will include surveillance of human esophageal tissues in patients with Barrett's esophagus. The transition to clinical usage will be facilitated by a newly developed version of a/LCI with a dramatically improved data acquisition time.[16]

References

1. L. M. Kalikin, A. Schneider, M. A. Thakur, Y. Fridman, L. B. Griffin, R. L. Dunn, T. J. Rosol, R. B. Shah, A. Rehemtulla, L. K. McCauley, and K. J. Pienta, "In vivo visualization of metastatic prostate cancer and quantitation of disease progression in immunocompromised mice," *Cancer Biol. Ther.* **2**(6), 656–660 (2003).
2. G. Choy, S. O'Connor, F. E. Diehn, N. Costouros, H. R. Alexander, P. Choyke, and S. K. Libutti, "Comparison of noninvasive fluorescent and bioluminescent small animal optical imaging," *BioTechniques* **35**(5), 1022–1026 (2003).
3. Y. Chen, G. Zheng, Z. H. Zhang, D. Blessington, M. Zhang, H. Li, Q. Liu, L. Zhou, X. Intes, S. Achilefu, and B. Chance, "Metabolism-enhanced tumor localization by fluorescence imaging: in vivo animal studies," *Opt. Lett.* **28**(21), 2070–2072 (2003).
4. A. Wax, C. H. Yang, M. G. Muller, R. Nines, C. W. Boone, V. E. Steele, G. D. Stoner, R. R. Dasari, and M. S. Feld, "In situ detection of neoplastic transformation and chemopreventive effects in rat esophagus epithelium using angle-resolved low-coherence interferometry," *Cancer Res.* **63**(13), 3556–3559 (2003).
5. H. K. Roy, Y. Liu, R. K. Wali, Y. L. Kim, A. K. Kromine, M. J. Goldberg, and V. Backman, "Four-dimensional elastic light-scattering fingerprints as preneoplastic markers in the rat model of colon carcinogenesis," *Gastroenterology* **126**(4), 1071–1081 (2004).
6. A. Wax, C. Yang, V. Backman, K. Badizadegan, C. W. Boone, R. R. Dasari, and M. S. Feld, "Cell organization and sub-structure measured using angle-resolved low coherence interferometry," *Biophys. J.* **82**, 2256–2264 (2002).
7. J. A. Izatt, M. D. Kulkarni, H. W. Wang, K. Kobayashi, and M. V. Sivak, "Optical coherence tomography and microscopy in gastrointestinal tissues," *IEEE J. Sel. Top. Quantum Electron.* **2**(4), 1017–1028 (1996).
8. D. Huang, E. A. Swanson, C. P. Lin, J. S. Schuman, W. G. Stinson, W. Chang, M. R. Hee, T. Flotte, K. Gregory, C. A. Puliafito, and J. G. Fujimoto, "Optical coherence tomography," *Science* **254**(5035), 1178–1181 (1991).
9. A. Wax, C. H. Yang, R. R. Dasari, and M. S. Feld, "Measurement of angular distributions by use of low-coherence interferometry for light-scattering spectroscopy," *Opt. Lett.* **26**(6), 322–324 (2001).
10. A. Wax, C. Yang, V. Backman, M. Kalashnikov, R. R. Dasari, and M. S. Feld, "Determination of particle size using the angular distribution of backscattered light as measured with low-coherence interferometry," *J. Opt. Soc. Am. A* **19**, 737–744 (2002).
11. J. W. Pyhtila, R. N. Graf, and A. Wax, "Determining nuclear morphology using an improved angle-resolved low coherence interferometry system," *Opt. Express* **11**(25), 3473–3484 (2003).
12. A. Wax and J. E. Thomas, "Optical heterodyne imaging and Wigner phase space distributions," *Opt. Lett.* **21**(18), 1427–1429 (1996).
13. A. J. Einstein, H. S. Wu, and J. Gil, "Self-affinity and lacunarity of chromatin texture in benign and malignant breast epithelial cell nuclei," *Phys. Rev. Lett.* **80**, 397–400 (1998).
14. R. S. Cotran, S. L. Robbins, and V. Kumar, *Robbins Pathological Basis of Disease*, Saunders, Philadelphia (1994).
15. L. Y. Y. Fong, V. T. Nguyen, A. E. Pegg, and P. N. Magee, "alpha-Difluoromethylornithine induction of apoptosis: a mechanism which reverses pre-established cell proliferation and cancer initiation in esophageal carcinogenesis in zinc-deficient rats," *Cancer Epidemiol. Biomarkers Prev.* **10**(3), 191–199 (2001).
16. J. W. Pyhtila and A. Wax, "Rapid, depth-resolved light scattering measurements using Fourier domain, angle-resolved low coherence interferometry," *Opt. Express* **12**, 6178–6183 (2004), http://www.opticsexpress.org/abstract.cfm?URI=OPEX-12-25-6178.